JOURNAL OF GEOPHYSICAL RESEARCH, VOL. 116, A02301, doi:10.1029/2010JA015958, 2011

Airglow observations and modeling of *F* region depletion zonal velocities over Christmas Island

Narayan P. Chapagain,[1] Michael J. Taylor,[1] and J. Vincent Eccles[2]

Received 22 July 2010; revised 20 October 2010; accepted 1 December 2010; published 3 February 2011.

[1] We report image measurements of plasma depletions in the equatorial *F* region ionosphere over Christmas Island (2.1°N, 157.4°W; dip latitude 2.8°N) in the central Pacific Ocean. The observations were made during the equinox period, September-October 1995, using a Utah State University CCD imaging system filtered to observe thermospheric O I (630.0 nm) airglow emissions centered at ~280 km altitude. Well-defined magnetic field-aligned depletions were observed on 18 nights during the campaign, including strong postmidnight fossilized structures, enabling detailed measurements of their morphology and dynamics. The number of depletions was influenced by their initial onset times and their persistence. The separations between adjacent depletions ranged from ~150 to ~250 km in good agreement with prior observations from other sites. However, measurements of their eastward zonal drift speeds indicated normal behavior peaking around 90–100 m/s prior to local midnight, with exceptionally high velocities, ~80 m/s during the postmidnight period that persisted until dawn. These results differ markedly from optical measurements at similar equatorial latitudes but at different longitude sectors, suggesting that the zonal drift velocities can have a significant longitudinal dependence. Model drift velocities calculated using a simple electric field model with winds defined by the horizontal wind model (HWM-07) produced an eastward drift throughout the night, but their postmidnight magnitudes were much smaller than observed. Using a modified HWM-07 wind field, a basic nighttime trend similar to the Christmas Island trend was successfully obtained.

Citation: Chapagain, N. P., M. J. Taylor, and J. V. Eccles (2011), Airglow observations and modeling of *F* region depletion zonal velocities over Christmas Island, *J. Geophys. Res.*, *116*, A02301, doi:10.1029/2010JA015958.

1. Introduction

[2] Optical observations of the nighttime *F* region equatorial ionosphere have been conducted from various low-latitude sites over the past three decades to study plasma irregularities associated with equatorial spread *F* (ESF) [e.g., *Weber et al.*, 1978; *Mendillo and Baumgardner*, 1982; *Sahai et al.*, 1994; *Taylor et al.*, 1997; *Kelley et al.*, 2002; *Makela et al.*, 2004]. These irregularities originate at or near the magnetic equator in the postsunset bottomside ionosphere and trigger the vertical development of plasma bubbles via the Rayleigh-Taylor instability (RTI). As the bubbles extend upward into the *F* region ionosphere, elongated magnetic north-south field-aligned structures of depleted plasma are created, which can map to dip latitudes greater than ±15° [e.g., *Maruyama*, 1988; *Rohrbaugh et al.*, 1989; *Sahai et al.*, 1994]. These structures are readily detected in the thermospheric O I (630.0 nm) airglow emissions as "equatorial depletions." They have zonal widths of typically a few tens of km and extend along the magnetic meridian for hundreds to thousands of km depending on the peak altitude of the irregularity (bubble) development, while their vertical heights range from a few tens of km to several hundred km [e.g., *Muralikrishna and Abdu*, 2006, and references therein].

[3] During its growth, the plasma velocity within a bubble is different from the ambient background plasma drift velocity. However, for fully developed, mature bubbles, the depletions move together with the background plasma drift as "fossilized" structures until the morning sunlight refills the depleted flux tubes due to enhanced ionization [e.g., *Makela et al.*, 2004]. The equatorial *F* region plasma depletion zonal velocity has proven to be an important parameter for the prediction of the occurrence of scintillations of satellite to ground RF signals [e.g., *Valladares et al.*, 2002]. The plasma drift velocity was first described by *Woodman* [1972] using radar measurements at Jicamarca, Peru (12°S, 76.9°W). Since then, extensive studies of plasma depletion zonal velocities have been conducted using a variety of techniques including ground-based radar, thermospheric airglow, and satellite measurements [e.g., *Fejer et al.*, 1991; *de Paula et al.*, 2002; *Pimenta et al.*, 2003a; *Sagawa et al.*, 2003; *Arruda et al.*, 2006]. These studies all

[1]Center for Atmospheric and Space Sciences, Utah State University, Logan, Utah, USA.
[2]Space Science Environment Corporation, Providence, Utah, USA.

0148-0227/11/2010JA015958

show that plasma bubbles propagate eastward during the nighttime (and rarely westward), under quiet magnetic conditions [e.g., *Taylor et al.*, 1997; *Abdu et al.*, 2003].

[4] Several studies obtained by different techniques have reported longitudinal variations in the development of plasma irregularities and their nocturnal zonal drift velocities [e.g., *Maruyama and Matuura*, 1984; *Immel et al.*, 2004; *Makela et al.*, 2004; *Jensen and Fejer*, 2007; *Pautet et al.*, 2009]. Of importance here are studies of plasma depletions in the Pacific sector, mainly using airglow measurements, with the earliest ground-based observations from Hawaii [20.7°N, 156.2°W] in the mid-1980s [*Rohrbaugh et al.*, 1989; *Tinsley et al.*, 1997]. Subsequently, *Kelley et al.* [2002] and *Makela et al.* [2004] reported on long-term measurements of the low-altitude thermosphere from Hawaii using an all-sky (180°) CCD imager and a colocated narrow field (47°) imager pointing southward along the magnetic meridian. In particular, they mapped depletions to apex heights of ~1500 km extending close to Christmas Island which is at the same geographic longitude but about 2000 km due south of Hawaii [*Kelley et al.*, 2002]. Using these instruments, *Yao and Makela* [2007] presented further equatorial plasma bubble zonal drift velocity measurements during 2002–2005 from Hawaii, while *Makela et al.* [2009] recently reported on low-latitude ionospheric events observed from Hawaii in coordination with 50 MHz coherent scatter radar measurements from Christmas Island.

[5] In this study, we report on observations of airglow depletions in equatorial *F* region ionosphere above Christmas Island in the central Pacific Ocean. The measurements were made during the autumnal equinox period (September 1995), using an all-sky CCD imager filtered to observe the thermospheric O I (630.0 nm) airglow emission. The derived zonal velocities were found to be unusually high during the postmidnight period (~80 m/s) as compared with previous results, mainly from different geographic longitudes. The effects of background thermospheric winds on zonal drift velocities are examined using the simple electric field model of *Eccles* [1998].

2. Observations and Data Analysis

[6] As part of a collaborative program with the Naval Postgraduate School, Monterey, CA, a Utah State University (USU) all-sky CCD airglow imager was set up and operated at Christmas Island, Republic of Kiritimati (2.1°N, 157.4°W, dip latitude 2.8°N) for a limited 1 month period from 15 September to 3 October 1995. The imager is a well-proven field instrument fitted with a sensitive back-thinned solid state 1024 × 1024 pixels CCD array and data were 2 × 2 binned on chip resulting in a zenith spatial resolution of 0.5 km. Sequential observations of the thermospheric O I (630.0 nm) airglow emission as well as the mesospheric near infrared (NIR) hydroxyl (OH) Meinel broad band emissions (710–930 nm) and the O I (557.7 nm) green line emissions were made using exposure times of 120 s, 15 s and 90 s, respectively. A background sky measurement was also recorded to discriminate between mesospheric and thermospheric structures and meteorological clouds. Further details of the all-sky instrument and its operational system are given by *Taylor et al.* [1995]. The main purpose of this campaign was to study the occurrence, spatial characteristics, and dynamics of the ionospheric plasma depletions and mesospheric gravity waves at equatorial latitudes.

[7] Figure 1 is a map of the Pacific region showing the central location of Christmas Island, about 2000 km due south of Hawaii. The open circle centered on Christmas Island represents the geographic field of view (FOV) of the all-sky imager (~1500 km diameter) for *F* region measurements, assuming a reference altitude of airglow emissions at 280 km appropriate for solar minimum conditions (average solar flux index $F_{10.7} \sim 73$). The enlarged airglow image below illustrates typical structure in the *F* region data recorded during this campaign. The dark bands in the image depict magnetic north-south aligned *F* region structures appearing as a series of depletions in the 630.0 nm airglow emission. These data have been used to study morphology and dynamics of equatorial depletions over Christmas Island.

[8] O I (630.0 nm) data were obtained from dusk to dawn throughout the moon down period using alternating time intervals of ~5 and ~11 min. resulting in typically 34–76 images per night. The observing conditions were good during this period and plasma depletions were measured on 17 occasions, with high contrast structures imaged on 15 of these nights. Although localized, intermittent cloud occasionally interfered with the time series observations, but they did not limit our ability to measure the motion of the depletions and their horizontal scale sizes during the course of each night.

[9] This analysis method is similar to that used by *Pimenta et al.* [2001] and is described further by *Pautet et al.* [2009]. The images were first calibrated using the known star field to determine the parameters of the imager such as its orientation and pixel scale size. The stars were then removed from the image sequences, which were subsequently unwarped (to correct for the all-sky lens format) [e.g., *Garcia et al.*, 1997], and projected onto a 1500 × 1500 km uniformly spaced geographic grid. The horizontal scale sizes of the structures were computed using a standard 2-D Fourier spectral analysis [e.g., *Taylor and Garcia*, 1995; *Garcia et al.*, 1997]. Drift speeds of individual depletions were then determined by selecting two sequential images, with time steps of ~16 min. Motion was measured at various positions along a given structure to determine its average velocity. This procedure was repeated for subsequent image pairs during the course of each night to determine the mean zonal drift speed of the plasma depletions as a function of local solar time.

[10] Figure 2 shows a time series of unwarped images of prominent *F* region structures recorded on 28–29 September. The left side axis plots magnetic latitude while the right side indicates geographic latitude, which extends from about 5°S to 9°N. On this occasion a faint broad depletion was first detected at 1957 LST and over the next hour the display evolved into several magnetic north-south aligned dark bands extending across the camera's FOV. Multiple depletion structures were observed over the next ~8 h (until dawn) moving steadily eastward, as indicated by the white arrows. On this occasion, the early evening structures comprised new depletions evolving in the vicinity of Christmas Island, as well as fully developed airglow depletions moving into the camera's FOV from the west. After local midnight, the depletions were dominated by fossilized structures progressing steadily eastward.

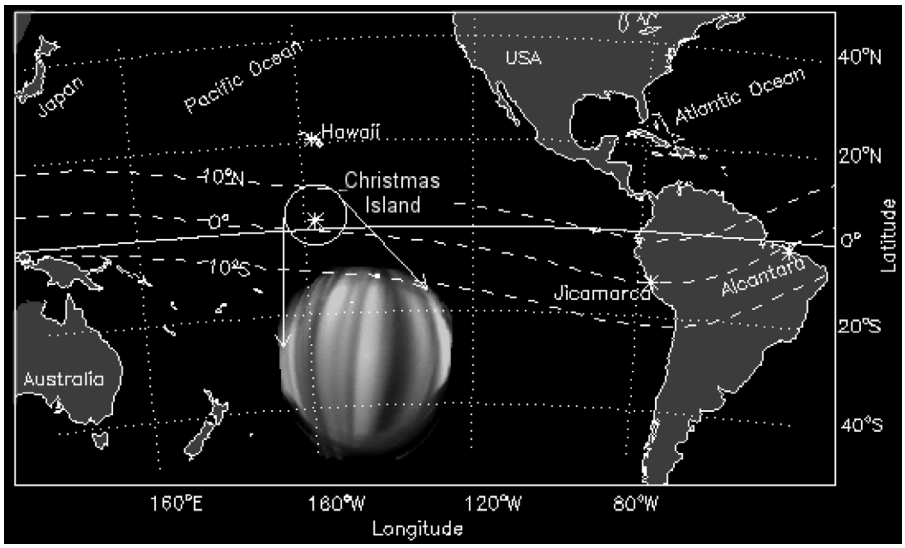

Figure 1. Map showing the central Pacific location of Christmas Island (2.1°N, 157°W), the field of view covered by the all-sky imager (circle), and an example of an O I (630.0 nm) airglow image. The dashed lines represent the dip latitudes at the magnetic equator, 10°S, and 10°N.

[11] Figure 3 contains data from several nights (in all-sky format) measured during the campaign and divided into premidnight and postmidnight periods. Nine nights of data are shown in each case. In the premidnight data (Figure 3a) each image was taken at approximately the same local solar time (2330 LST) to compare depletion activity and spatial characteristics. Although some night-to-night variability is evident in the number of depletions and their spatial separations, all of the images contain well-developed, extensive field-aligned structures by this time. This situation prevailed for 15 nights. The depletions were numerous and exhibited the highest eastward drift speed during this period (see section 3.3). In comparison, Figure 3b shows nine examples of the postmidnight depletion activity imaged between 0100 and 0440 LST. These data contained mainly fossilized structures that appeared fully developed when they entered into the camera's FOV. They exhibited little change in their east-west dimensions as they drifted eastward and often persisted until dawn. Together, these data illustrate the strong and persistent *F* region activity recorded during this equinox period.

3. Results

[12] These high-quality image data have been used to investigate several key characteristics of the plasma depletions observed from Christmas Island.

3.1. Depletion Occurrence, Onset, and Duration

[13] Figure 4 (top) plots the number of plasma depletions observed on each night during the campaign. A large day-to-day variation is evident in their total number which ranged from 1 to 14 per night. As mentioned earlier, some of the nights were intermittently cloudy, but this did not restrict our ability to determine the number, and duration of the depletions. For example, their low occurrence on UT days 262, 263 and 266 (indicated by the vertical dotted lines) was not due to limited sky conditions.

[14] Figure 4 (middle) plots the initial onset times of the depletions that were observed to grow inside the field of view of the camera (mainly to the west of Christmas Island). During most of the nights the onset time of these plasma structures occurred in the early evening around 1930 to 2030 LST, which is consistent with previous climatological results obtained from radar observations of ESF from Jicamarca, Peru recently reported by *Chapagain et al.* [2009]. For comparison, Figure 4 (bottom) plots the estimated duration of the depletions for each night. Together these three plots show that the total number of depletion structures observed was strongly influenced by their initial onset time and persistence. Figure 4 clearly illustrates that the number of depletions was large when their onset was early and their observed duration was long (~9–10 h). For example, on UT day 269 (26–27 September) the onset time was ~1930 LST and 14 structures were observed during the course of the night (indicated by the solid vertical line). In contrast, on nights when only a few depletions were observed (indicated by the dotted lines), their onset time was ~1 h later and plasma structures persisted for a relatively short period of time, ~2–5 h.

3.2. Horizontal Scale Size of the Depletions

[15] The magnetic field-aligned structures observed over Christmas Island (e.g., Figure 2) exhibited a range of zonal separations that differed during the course of a night, and from night to night. Similar morphology structures were observed by the USU camera a year earlier from Alcantara, Brazil (2.3°S, 44.4°W, dip latitude 6.7°S) during the NASA-INPE Guara Campaign [*Taylor et al.*, 1997]. Figure 5 plots the distribution of the zonal distance between adjacent depletions observed during the campaign. The separations ranged from as little as several km up to 550 km but were most frequently spaced 100–250 km apart. (Note, the minimum separation between the structures reported in this plot was 25 km.) For comparison the results from Alcantara, Brazil (October 1994) under similar solar minimum

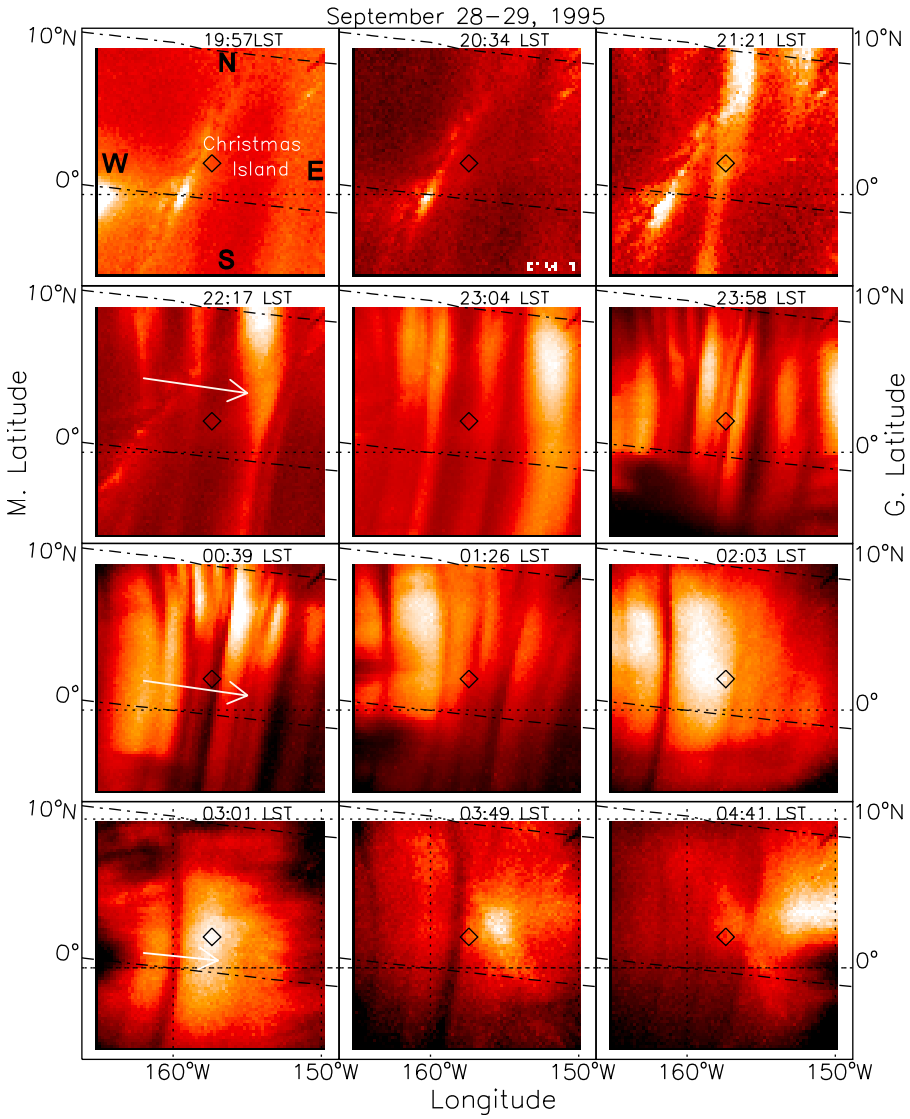

Figure 2. Sequence of unwarped all-sky O I (630.0 nm) airglow images showing the spatial characteristics and time evolution of a series of depletions (dark bands) imaged on 28–29 September 1995, from ~2000 to 0440 local solar time (LST). The dash-dotted lines indicate the magnetic equator (0°) and magnetic latitude at 10°N. The time difference between LST at Christmas Island and universal time (UT) is 10.5 h.

conditions were also plotted. The Brazilian observations were more limited by clouds, but both data sets revealed similar dominant scale sizes for their zonal separations, ranging from ~150–250 km over Christmas Island (42% of events), and ~100–200 km over Alcantara (~52% of events). These results are consistent with the recent depletion measurements (dominant separations ~100–200 km) from Brazil (dip latitude ~10°) under similar solar minimum conditions reported by *Pautet et al.* [2009].

3.3. Overview of Depletion Evolution and Motion

[16] Figure 6 shows two keogram plots summarizing the evolution, development, and propagation of depletions observed on two nights (18–19 and 28–29 September) during the campaign. The plots were made by taking a horizontal (west-east) slice passing through the zenith of each unwarped image. The data were then spliced together to create a time series showing the zonal development of the depletions observed on both of these nights. Although keogram plots lose much of the two-dimensional spatial information present in the original images, they provide an important overview of depletion activity during the night. The dark bands progressing in time from the bottom left to the top right (i.e., from west to east) show the onset and subsequent motion of several depletions, as indicated by the arrows. The near-linear slopes of these bands, which give the depletion zonal drift velocity in the geographic frame, indicate that they were moving with almost constant, but different magnitude of velocities, on these two occasions.

[17] On 18–19 September, the first two depletions appeared to develop within the camera's field prior to ~2030 LST, subsequently, other already well-developed structures entered the FOV. The slopes of all of the depletions indicate a zonal velocity of ~70–80 m/s throughout the

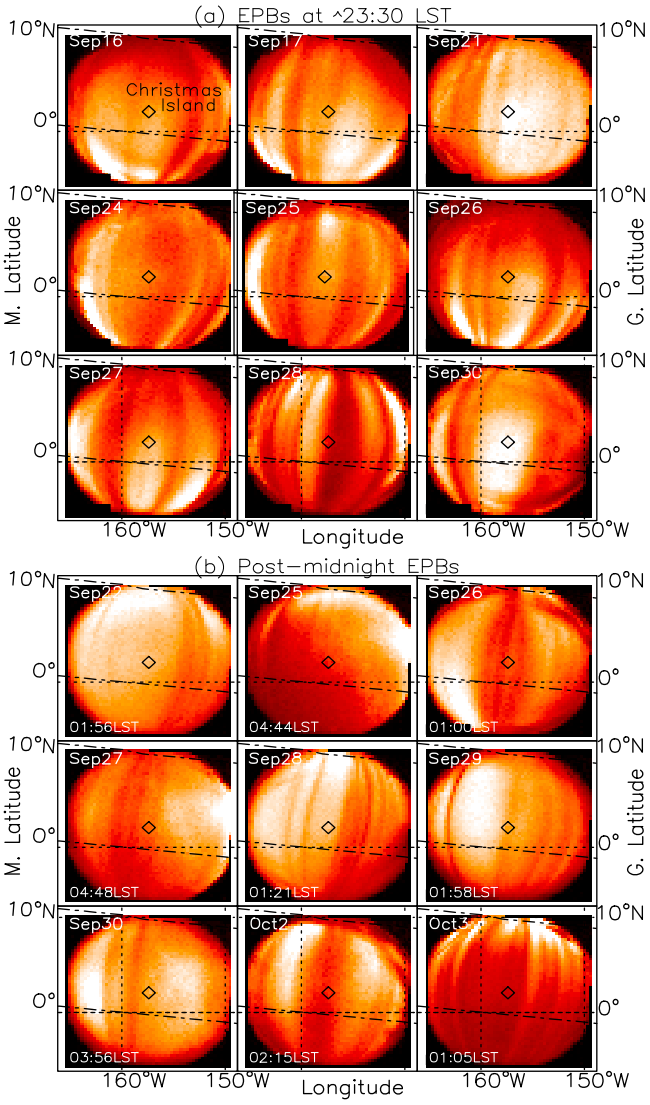

Figure 3. Comparison of depletions imaged over Christmas Island for the (a) premidnight and (b) postmidnight periods. Strong depletion structures were observed on all clear nights prior to midnight, while fossilized structures were occasionally observed until the dawn.

night. Around local solar midnight, the leading structures exited the camera's FOV, while subsequent depletions began to fade. On 28–29 September, a similar situation occurred, and multiple structures were observed to evolve inside the FOV, but somewhat later, around 2200 LST. These depletions then moved steadily eastward with a higher constant velocity (~90–110 m/s), and persisted longer, at least until ~0200 LST when they exited the camera's FOV to the east. A single isolated structure was also observed during the postmidnight period until dawn, again moving steadily eastward, but with a lower velocity (~60 m/s). Similar trends for the depletion motions were observed during most of the nights from Christmas Island, as described below.

3.4. Depletion Zonal Velocities

[18] The zonal velocities of the individual plasma depletions as a function of LST were measured on 17 near-

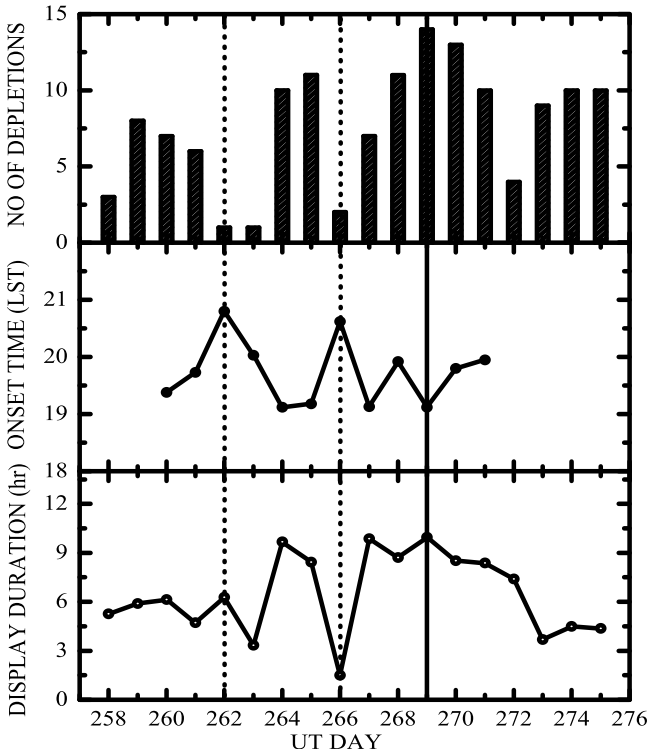

Figure 4. (top) The total number of depletion structures observed each night, (middle) the onset time of the depletions over Christmas Island, and (bottom) their nocturnal duration.

consecutive nights. As described in section 2, the unwarped images were used to determine an average drift velocity for each depletion structure. Drift velocities were usually calculated from structures as they moved through the zenith sky. However, these data were often supplemented by measurements of depletions closer to the edges of the camera's FOV and were adjusted to the same LST. Figure 7 plots the

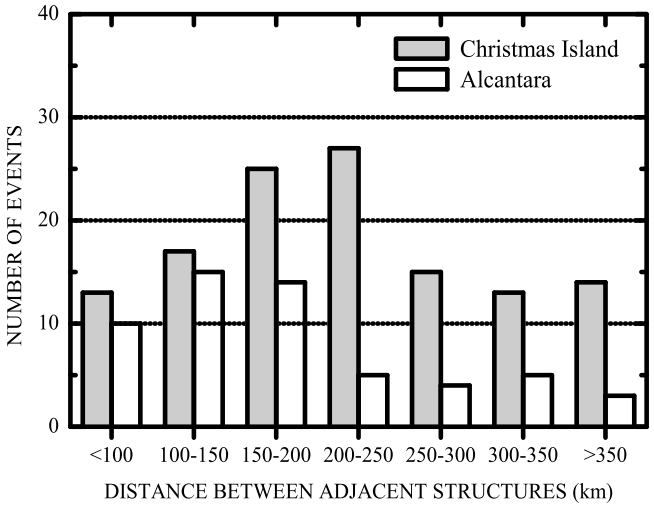

Figure 5. Histogram plots of the distance between two consecutive plasma depletions observed over Christmas Island and Alcantara, Brazil.

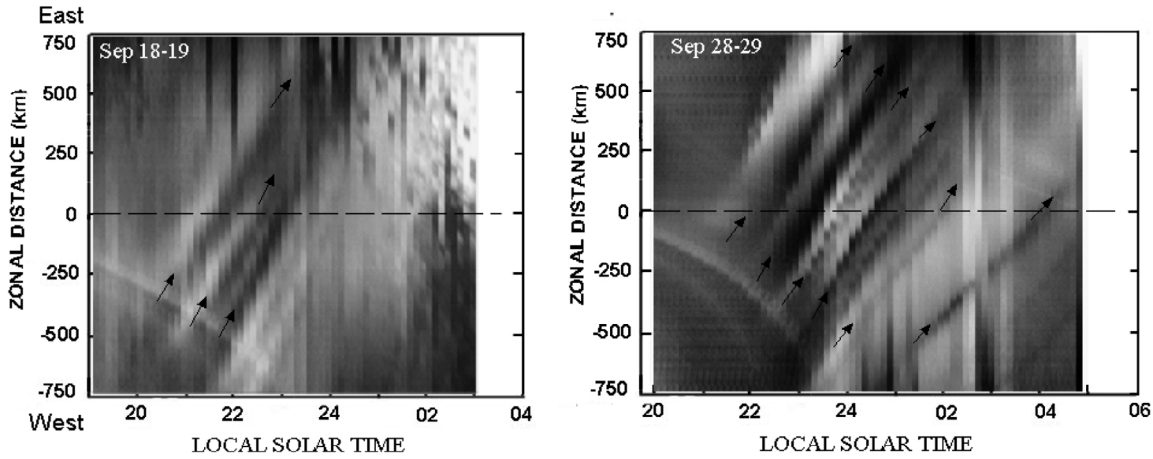

Figure 6. Example keogram plots summarizing the west-east (zonal) evolution of depletions observed on two occasions from Christmas Island. The arrows show the direction of motion of the plasma depletions (dark bands), while their slopes indicate almost constant zonal velocities during the nights. In each plot, the curved band in the bottom left is due to the passage of the Milky Way (which was not fully removed during the image processing), while the horizontal dashed line indicates the zenith.

derived zonal velocities of 14 consecutive depletions observed on 28–29 September as a function of LST. The embedded O I image shows several examples of depletions at 2351 LST (numbered 1–7). The drift velocities of each structure overlap very well. The average velocity, indicated by the bold line, peaked at ~115 m/s around 2300 LST and then decreased over the next ~2 h down to ~60 m/s, and thereafter remained approximately constant until dawn at ~0445 LST.

[19] Using the above procedure, Figure 8 summarizes the average depletion zonal velocities (17 nights) as a function of LST. While the individual plots show significant night-to-night variability in the derived depletion drift velocities, the data ensemble show good temporal coverage (from ~1900 to 0500 LST) during the campaign, with a clear nocturnal signature. This is indicated by the bold curve, which plots the average velocity of all measurements while the vertical bars indicate their standard deviations (up to 38 m/s) from this mean. Limited observations shortly after dusk (~1900 LST) revealed very low eastward, ~7 m/s (26–27 September) and even westward, ~20 m/s (24–25 September) drifts. By 2030 LST, multiple observations show that the average zonal velocity then increased rapidly during the early evening hours and peaked around 2130–2300 LST with a mean value ~90 m/s (with individual velocities up to 125 m/s). The average drift velocity then decreased slightly to ~80 m/s by midnight LST and thereafter remained approximately constant over the next ~5 h

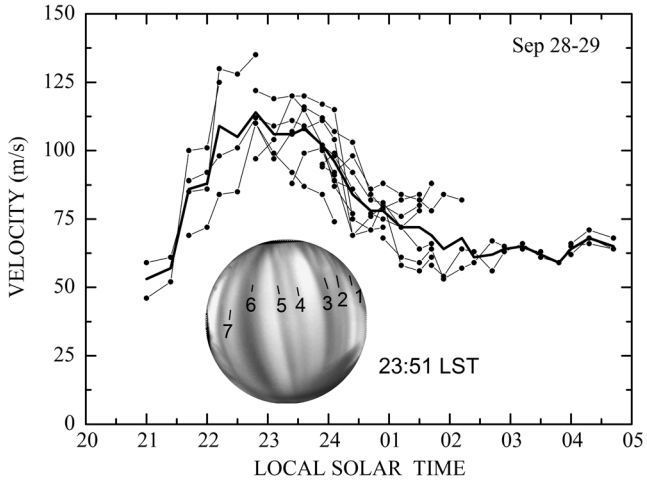

Figure 7. Depletion drift velocities for several consecutive structures during the night of 28–29 September. Examples of depletion numbers (1, 2, 3, 4, 5, etc.) are also shown in the O I image at 2351 LST. The bold line represents the averaged velocity of all depletions.

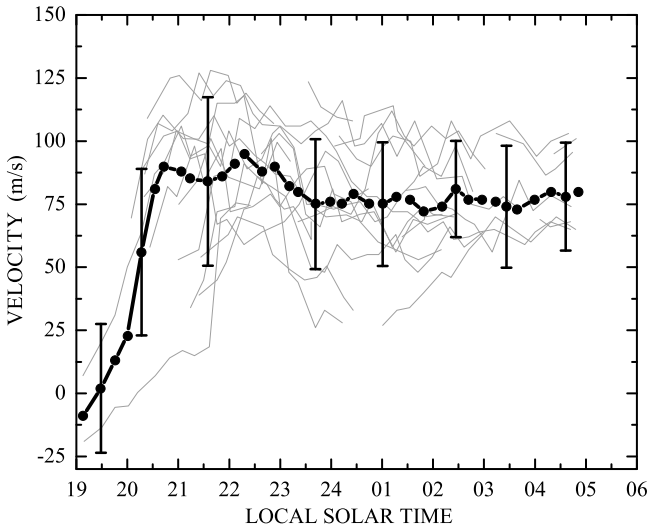

Figure 8. The average depletion velocities for all 17 nights of the campaign calculated from two successive images for time binned at ~16 min. Bold data points represent averaged velocity, and the vertical bars are the standard deviations from the mean. The average solar flux index ($F_{10.7}$ cm) is 73.

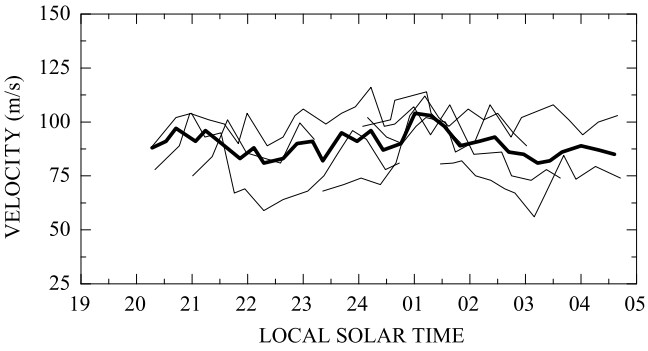

Figure 9. Superposition of velocity plots for six nights of the campaign that remained nearly constant throughout the night. The bold line represents the average velocity.

until dawn. This describes the overall behavior of the zonal drift velocity, however, on at least 6 nights during the campaign, no peak was detected and instead the drift velocity remained almost constant throughout the night (from 2030 to 0430 LST) with a high mean value of ~90 m/s. For comparison, these data are plotted in Figure 9 to illustrate the unusual nature. In general, the average premidnight velocity results agree well with previous ground-based measurements in equatorial regions under similar solar minimum conditions [e.g., *Fejer et al.*, 1991; *Taylor et al.*, 1997; *Valladares et al.*, 2002; *de Paula et al.*, 2002; *Martinis et al.*, 2003] however, the postmidnight velocities were significantly higher.

[20] Finally, to examine the influence of the magnetic activity on zonal drift during campaign, we checked the average value of the 3-hourly geomagnetic index (Kp) over a 9 h period (1330–2230 LST). This time interval includes 6 h prior to local sunset during which depletion onset may be influenced by geomagnetic storms. However, the geomagnetic activity was quiet (Kp < 3) except during 2 days when Kp was slightly larger than 3, and no significant difference in the depletion activity was evident. This result was to be expected as geomagnetic storms during solar minimum conditions are known not to significantly affect the zonal drift velocities [e.g., *Fejer et al.*, 2005].

4. Discussion

4.1. Characteristics in the Christmas Island Airglow Structures

[21] The depletions observed from Christmas Island are clearly similar to O I (630.0 nm) thermospheric observations from other sites at equatorial and low latitudes. Their magnetic meridian alignment, sharp east-west gradients in the airglow structure and spacing of the dark bands strongly suggest that they are the airglow signature of the medium-scale field-aligned plasma bubbles generated by the R-T instability. Studies of ESF irregularities using Atmospheric Explorer E (AE-E) plasma density measurements reported that the irregularities have the form of sharp quasiperiodic depletions [e.g., *Tsunoda et al.*, 1982; *Hysell and Kelley*, 1997]. *Abalde et al.* [2001] presented the fine structure of the quasi field-aligned ionospheric plasma bubbles using the O I 777.4 nm emission image measurements. Since the Christmas Island observations were from close to the dip equator, the results only show the airglow structure of the bottomside *F* region modulations in the plasma depletions. Therefore, these data cannot demonstrate that these *F* region plasma bubble structures penetrated to the topside ionosphere, though they likely did. Particularly in the early evening, some structures may only have been bottomside modulations, yet to grow into topside bubbles. Most of the nights, the depletions developed in the FOV of the camera during early evening and then drifted eastward. They are seen close to 1930 LST (1 h after ground level local sunset) to 0400 LST (0930 h after local sunset). Thus, these early evening plasma depletions and possible plasma bubbles have their initial development near Christmas Island longitude. Later in the evening airglow signatures of depletions forming at other longitudes drifted into the FOV as fossil depletions just as observed by *Makela et al.* [2004]. The airglow signatures of the fossil structures sometimes will remain until local sunrise when the sun reionizes the ionosphere.

4.2. Longitudinal and Latitudinal Characteristics of the Zonal Drifts

[22] In Figure 10 we compared the average depletion zonal velocities from Christmas Island with previous optical observations from Haleakala, Hawaii (20.7°N, 157.2°W, dip latitude 21°N) [*Yao and Makela*, 2007], and Alcantara, Brazil (2.3°S, 44.5°W, dip latitude 6.7°S) [*Taylor et al.*, 1997], all of which were obtained under similar low solar flux conditions. The smooth curve plots the empirical model results derived from Jicamarca radar measurements from 1970 to 2003, Peru (12°S, 76.9°W, dip latitude 1°N) also for low solar flux conditions (average $F_{10.7}$ = 90) [*Fejer et al.*, 2005]. Figure 10 shows that the local time dependence of the depletion zonal velocities prior to midnight LST were quite similar from Christmas Island and Haleakala, which are almost at the same longitude but separated in latitude

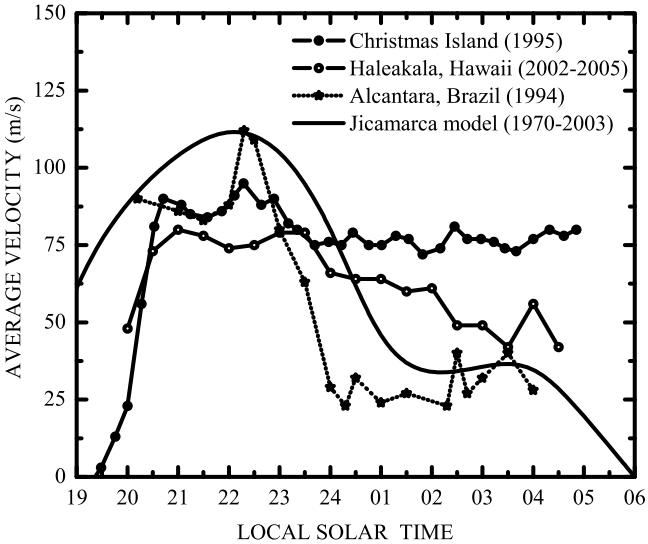

Figure 10. Comparison of the average airglow depletion zonal velocities from Christmas Island with previous observations (replotted) from Haleakala, Hawaii [*Yao and Makela*, 2007], and Alcantara, Brazil [*Taylor et al.*, 1997], and empirical model of the plasma drift velocities derived from the radar measurement (replotted) from Jicamarca, Peru [*Fejer et al.*, 2005].

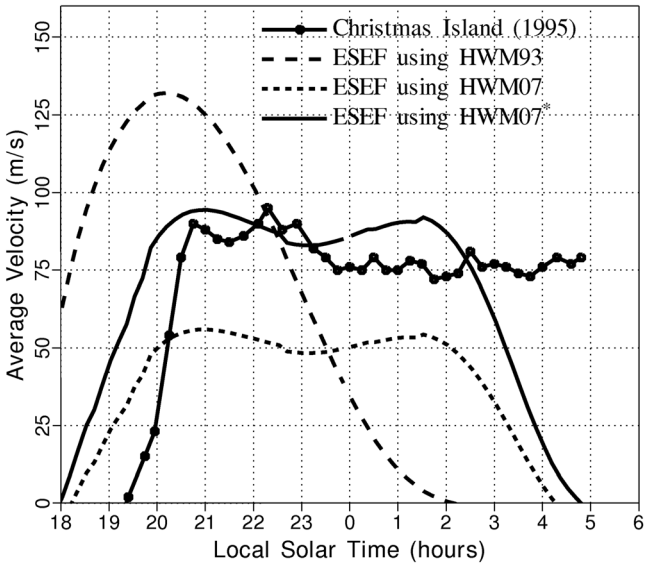

Figure 11. Average zonal drifts at 280 km above Christmas Island for equinox of 1995 comparing average observations with the ESEF model results using various wind models.

by ~20°. Furthermore, the premidnight Christmas Island drift velocities are consistent with the measurements from Alcantara, Brazil (obtained a year earlier), and the Jicamarca climatological model results with drift velocities peaked at ~110 m/s within the observed range of measurements reported herein (see Figure 8). However, it is clear that the Christmas Island postmidnight velocities remained elevated in magnitude over the postmidnight drifts of the previous studies.

[23] The depletion zonal drift observations at Christmas Island and Alcantara, Brazil (Figure 10) are both near the dip equator, but exhibited very different zonal drifts throughout the night. Similarly, the plasma zonal drift model from Jicamarca Radar observations are also at the dip equator in the American longitude sector. Alcantara and Jicamarca lines in Figure 10 show strong deceleration of the zonal drifts around local midnight. The differences in average zonal plasma drift of Christmas Island and the results from the South American sector suggest significant differences between their longitude sectors such as dip equator offset, declination, and neutral winds. Satellite studies have also reported a longitudinal dependence of zonal drifts velocities [e.g., *Immel et al.*, 2004; *Jensen and Fejer*, 2007].

[24] There are several possible reasons for the differing magnitudes of the background zonal plasma drifts between our results and those presented in the airglow studies at other longitudes. For example, we have calculated the velocities at an assumed emission altitude of 280 km of the O I (630.0 nm) airglow images. It has been shown that the velocities calculated at an assumed emission height of 300 km are up to 20% higher than that of 250 km [*Pimenta et al.*, 2003b]. This also will cause the differences in the magnitude of the drift velocities from other locations but does not alter the time history during the course of the night. The Christmas Island result of a nearly constant elevated zonal drift history is strong evidence of longitudinal differences in the winds or electrodynamics resulting in different nighttime zonal drifts.

[25] The drift velocities were larger throughout the night than drifts observed from Haleakala in the same longitude sector. The apex altitudes corresponding to the FOV of the imager at Christmas Island cover approximately from 280 to 450 km, whereas at Haleakala corresponds to at higher altitudes (up to ~950 km) [*Yao* and *Makela*, 2007]. The zonal plasma drift does vary with altitude in the early evening hours in particular, and also throughout the night [*Eccles*, 1998; *Fejer et al.*, 2005]. Christmas Island and Haleakala observations may also demonstrate this latitudinal (or altitudinal) variations of the zonal drift velocity. *Martinis et al.* [2003] and *Pimenta et al.* [2003a] use airglow observations to show that ion drag from equatorial ionosphere anomaly cause thermospheric neutral wind and therefore plasma drift velocities to have latitudinal dependence in which velocities decrease with increasing latitude. This is supported by the average zonal drifts of Christmas Island and Haleakala, Hawaii plotted in Figure 10.

4.3. Early Evening Drifts

[26] In the early evening the average zonal drifts prior to 2030 LST were substantially lower in magnitude from the average plasma drifts of those seen by *Fejer et al.* [2005]. These early evening drifts are from the two nights of observations (as shown in Figure 8). The Haleakala observations similarly show a late acceleration after sunset. The zonal drift model of *Fejer et al.* [2005] is based on Jicamarca Radar drift observations of the *F* peak plasma. Airglow depletion zonal drifts are indicators of *F* region bottomside drifts. The observed airglow depletion drifts prior to 2030 LST might be associated with the postsunset plasma flow vortex below the *F* layer peak [*Haerendel et al.*, 1992; *Eccles et al.*, 1999; *Kudeki and Bhattacharyya*, 1999]. The vertical rise and fall of the ionosphere near local sunset is accompanied by westward flow in the lower altitudes and eastward flow above. The null velocity of the zonal flow shear rises with the *F* region [*Haerendel et al.*, 1992]. The vortex flow has been reported in satellite observations [*Eccles et al.*, 1999] and in radar backscatter observations [*Kudeki and Bhattacharyya*, 1999]. The backscatter figures of *Kudeki and Bhattacharyya* [1999] indicate that the bottomside irregularities after sunset are embedded in the bottom of the *F* region where the flow is westward (<300 km). The early evening plasma plume signatures in the O I (630.0 nm) airglow from these 2 days of observations may have been embedded in the *F* region, near the null of the shear in the zonal plasma flow. The altitude of the drift shear began to descend with the ionosphere around 1930 LST. This descent of the *F* region, the shear, and the embedded plasma structures is seen in Plate 2 of *Kudeki and Bhattacharyya* [1999]. The descent of the shear should eventually embed the airglow structures in the eastward drifting plasma.

[27] *Martinis et al.* [2003] investigated the dependence of the zonal airglow depletion drifts with latitude and found that the early postsunset zonal drifts near the magnetic equator are influenced by the *E* layer dynamo, while the equatorial anomaly region zonal drifts are dominated by the *F* layer dynamo. These results agree with our interpretation of the early evening drift discrepancy of the Christmas Island observations and the *Fejer et al.* [1991] *F* region zonal drifts.

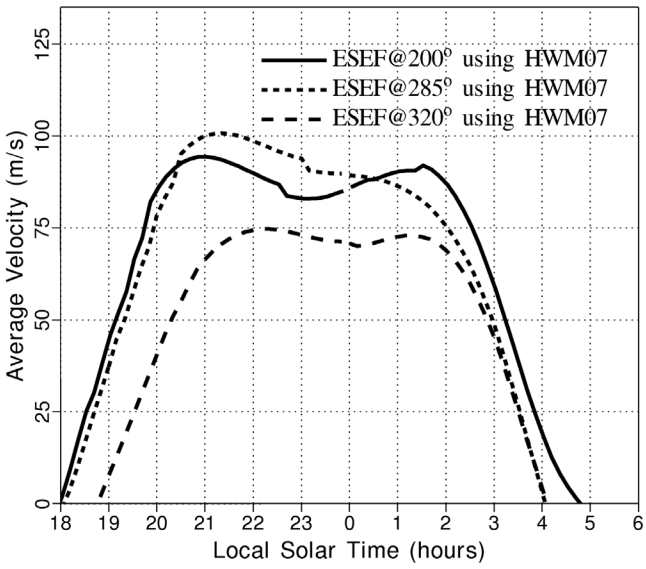

Figure 12. Plot of the ESEF results for three longitude sectors: Christmas Island (200°E), Peru (285°E), and Brazil (320°E).

4.4. Plasma Drift Modeling

[28] These results are now compared with a physics-based model of low-latitude drifts using field line-integrated electrodynamics. The Eccles Simple Electric Field model [*Eccles*, 1998] (hereafter referred to as ESEF) is a simplified electric field model that combines a specification of the ionosphere, thermosphere density, and thermospheric winds in a single magnetic meridian to produce the low-latitude *F* region electric fields using field line-integrated quantities [*Haerendel et al.*, 1992; *Eccles*, 1998]. The ESEF model provides field line-integrated conductivities and plasma drifts for apex altitudes from 200 to ~1000 km, based on underlying empirical models. The ESEF results have been tested against the fully global electric field model with nearly identical results for *F* region plasma drifts. This simple model can be run in minutes on a single CPU computer by focusing on a single sector rather than solving the entire globe. This allows us to investigate the effects of *F* region winds on the observed electric fields.

[29] For this study we have used the International Reference Ionosphere (IRI) [*Bilitza and Reinisch*, 2008], the MSIS-90 model atmosphere [*Hedin*, 1991], and several horizontal wind model (HWM) versions. The neutral wind model is of key importance to the electric field calculation. The HWM90 [*Hedin et al.*, 1991] and HWM93 [*Hedin et al.*, 1996] versions were both used for the zonal drift calculations, but they proved to give nearly identical results. Only the HWM93 results are presented here. The new HWM 2007 version [*Drob et al.*, 2008] was also used in this study. Figure 11 presents the model results for the prevailing conditions of the Christmas Island observations (solid line with symbols). The two dashed lines show the computed zonal plasma drifts from the ESEF model using the HWM models without modification. The HWM93 data (long dash) provides neutral winds that drive strong eastward (positive) plasma drift early in the evening, but the rapid drop to very low drift values around midnight LST is not representative of our measurements. In contrast, the HWM07 data (short dash) maintains an eastward drift throughout the night, but the magnitude of the drift velocities is much smaller than observed.

[30] The HWM07 winds should be appropriate for the solar minimum conditions of observations, but this study suggests that the magnitude of the zonal neutral winds are too small by half when the ESEF model drifts are compared to the Christmas Island plasma drift observations. As a simple experiment we have modified the HWM07 winds using a least squares minimization between the model and the averaged drift velocity data. It was assumed that the form of the HWM07 winds in local, altitude, and latitude remained the same. The zonal winds (u_s) were multiplied by a factor and a constant offset was added to the scaled zonal component:

$$u_s^* = au_s + b$$

where u_s is the zonal wind of the HWM07 model and u_s^* is the modified zonal wind. The coefficients, a and b, are constants. Only the eastward wind was given an offset as an average super rotation adjustment to the zonal wind. The solid line in Figure 11 plots the results of the zonal plasma drifts derived from the ESEF using the optimally modified HWM07. (A reasonable choice for the values of the coefficients were a = 1.5 and b = 10 m/s.) The model results now show good overall agreement with the Christmas Island observations.

[31] Figure 12 investigates the effects of longitudinal variations in the HWM07 equatorial winds and the IGRF magnetic field on the resulting zonal plasma drifts. We model three longitude sectors: Christmas Island, Peru, and Brazil. The resulting zonal drifts demonstrate that the HWM07 winds provide a basic nighttime trend similar to Christmas Island, but other longitude results do not differ significantly from the Christmas Island results even though the magnetic field declination and dip equator latitude have large differences between these longitude sectors.

5. Conclusions

[32] We have presented observations of nighttime airglow depletions from Christmas Island using all-sky images of the thermospheric O I (630.0 nm) airglow emissions. The magnetic field-aligned depletions were most likely associated with the development of EPBs and were observed on every night of the campaign. The airglow depletions mostly developed during ~1930–2000 LST and their active growth region was close to the west edge of camera's FOV suggesting that they were seeded to the west of Christmas Island. The number of depletions was well correlated with their initial onset times and their persistence. The spacing between structures ranged mostly from ~150 to 250 km, which is similar to the equatorial observation from other longitudes.

[33] Measurements of depletion drift velocities from Christmas Island were eastward and exhibited significantly day-to-day variations in their magnitudes. The average velocity peaked around 90–100 m/s approximately 2 h after local sunset and remained at a nearly constant high value ~80 m/s during the postmidnight period until dawn. This postmidnight elevated eastward drift differs significantly from prior observations at other longitudes.

[34] The ESEF drift model was used to investigate the zonal plasma drifts over Christmas Island using wind fields from existing empirical models (HWM-93 and HWM-07). The model results from the HWM07 wind model produced an eastward drift throughout the night but their postmidnight magnitudes were much smaller than observed. Using a modified HWM-07 wind field a basic nighttime trend similar to the Christmas Island was successfully obtained.

[35] The apparent longitudinal dependence of equatorial depletion drift velocities is clearly of interest. Future studies using multiple stations at closely spaced longitudes (as recently conducted from equatorial Brazil) together with satellite observations such as those of currently being made by the U.S. Air Force Communication/Navigation Outage Forecasting System (C/NOFS) satellite will provide crucial data for understanding longitudinal variability.

[36] **Acknowledgments.** This research was supported as part of a collaborative study with the Naval Postgraduate School, Monterey, California, to whom we are most grateful. Modeling studies were supported by the NSF contract 0745714.

[37] Robert Lysak thanks Takashi Maruyama and another reviewer for their assistance in evaluating this paper.

References

Abalde, J. R., P. R. Fagundes, J. A. Bittencourt, and Y. Sahai (2001), Observations of equatorial *F* region plasma bubbles using simultaneous OI 777.4 nm and OI 630.0 nm imaging: New results, *J. Geophys. Res.*, *106*(A12), 30,331–30,336, doi:10.1029/2001JA001115.

Abdu, M. A., J. R. de Souza, I. S. Batista, and J. H. A. Sobral (2003), Equatorial spread *F* statistics and empirical representation for IRI: A regional model for the Brazilian longitude sector, *Adv. Space Res.*, *31*, 703–716, doi:10.1016/S0273-1177(03)00031-0.

Arruda, D. C. S., J. H. A. Sobral, M. A. Abdu, V. M. Castilho, H. Takahashi, A. F. Medeiros, and R. A. Buriti (2006), Theoretical and experimental zonal drift velocities of the ionospheric plasma bubbles over the Brazilian region, *Adv. Space Res.*, *38*, 2610–2614, doi:10.1016/j.asr.2006.05.015.

Bilitza, D., and B. Reinisch (2008), International reference ionosphere 2007: Improvements and new parameters, *Adv. Space Res.*, *42*, 599–609, doi:10.1016/j.asr.2007.07.048.

Chapagain, N. P., B. G. Fejer, and J. L. Chau (2009), Climatology of post-sunset equatorial spread *F* over Jicamarca, *J. Geophys. Res.*, *114*, A07307, doi:10.1029/2008JA013911.

de Paula, E. R., et al. (2002), Ionospheric irregularity zonal velocities over Cachoeira Paulista, *J. Atmos. Sol. Terr. Phys.*, *64*, 1511–1516, doi:10.1016/S1364-6826(02)00088-3.

Drob, D. P., et al. (2008), An empirical model of the Earth's horizontal wind fields: HWM07, *J. Geophys. Res.*, *113*, A12304, doi:10.1029/2008JA013668.

Eccles, J. V. (1998), A simple model of low-latitude electric fields, *J. Geophys. Res.*, *103*(A11), 26,699–26,708.

Eccles, J. V., N. Maynard, and G. Wilson (1999), Study of the evening plasma drift vortex in the low-latitude ionosphere using San Marco electric field measurements, *J. Geophys. Res.*, *104*(A12), 28,133–28,143, doi:10.1029/1999JA900373.

Fejer, B. G., E. R. de Paula, S. A. Gonzalez, and R. F. Woodman (1991), Average vertical and zonal *F* region plasma drifts over Jicamarca, *J. Geophys. Res.*, *96*(A8), 13,901–13,906, doi:10.1029/91JA01171.

Fejer, B. G., J. R. Souza, A. S. Santos, and A. E. Cost Pereira (2005), Climatology of *F* region zonal plasma drifts over Jicamarca, *J. Geophys. Res.*, *110*, A12310, doi:10.1029/2005JA011324.

Garcia, F. J., M. J. Taylor, and M. C. Kelley (1997), Two-dimensional spectral analysis of mesospheric airglow image data, *Appl. Opt.*, *36*(29), 7374–7385, doi:10.1364/AO.36.007374.

Haerendel, G., J. V. Eccles, and S. Cakir (1992), Theory for modeling the equatorial evening ionosphere and the origin of the shear in the horizontal plasma flow, *J. Geophys. Res.*, *97*(A2), 1209–1223, doi:10.1029/91JA02226.

Hedin, A. (1991), Extension of the MSIS thermosphere model into the middle and lower atmosphere, *J. Geophys. Res.*, *96*(A2), 1159–1172, doi:10.1029/90JA02125.

Hedin, A., et al. (1991), Revised global model of thermosphere winds using satellite and ground-based observations, *J. Geophys. Res.*, *96*(A5), 7657–7688, doi:10.1029/91JA00251.

Hedin, A., et al. (1996), Empirical wind model for the upper, middle and lower atmosphere, *J. Atmos. Terr. Phys.*, *58*, 1421–1447, doi:10.1016/0021-9169(95)00122-0.

Hysell, D. L., and M. C. Kelley (1997), Decaying equatorial *F* region plasma depletions, *J. Geophys. Res.*, *102*(A9), 20,007–20,017, doi:10.1029/97JA01725.

Immel, T. J., H. U. Frey, S. B. Mende, and E. Sagawa (2004), Global observations of the zonal drifts speed of equatorial ionospheric plasma bubbles, *Ann. Geophys.*, *22*, 3099–3107, doi:10.5194/angeo-22-3099-2004.

Jensen, J. W., and B. G. Fejer (2007), Longitudinal dependence of middle and low latitude zonal plasma drifts measured by DE-2, *Ann. Geophys.*, *22*, 2551–2559.

Kelley, M. C., J. J. Makela, B. M. Ledvina, and P. M. Kintner (2002), Observations of equatorial spread *F* from Haleakala, Hawaii, *Geophys. Res. Lett.*, *29*(20), 2003, doi:10.1029/2002GL015509.

Kudeki, E., and S. Bhattacharyya (1999), Postsunset vortex in equatorial *F* region plasma drifts and implications for bottomside spread *F*, *J. Geophys. Res.*, *104*(A12), 28,163–28,170, doi:10.1029/1998JA900111.

Makela, J. J., B. M. Ledvina, M. C. Kelley, and P. M. Kintner (2004), Analysis of the seasonal variations of equatorial plasma bubble occurrence observed from Haleakala, Hawaii, *Ann. Geophys.*, *22*, 3109–3121, doi:10.5194/angeo-22-3109-2004.

Makela, J. J., M. C. Kelley, and R. T. Tsunoda (2009), Observations of midlatitude ionospheric instabilities generating meter-scale waves at the magnetic equator, *J. Geophys. Res.*, *114*, A01307, doi:10.1029/2007JA012946.

Martinis, C., J. V. Eccles, J. Baumgardner, J. Manzano, and M. Mendillo (2003), Latitude dependence of zonal plasma drifts obtained from dual site airglow observations, *J. Geophys. Res.*, *108*(A3), 1129, doi:10.1029/2002JA009462.

Maruyama, T. (1988), A diagnostic model for equatorial spread *F*: 1. Model description and application to electric field and neutral wind effects, *J. Geophys. Res.*, *93*(A12), 14,611–14,622, doi:10.1029/JA093iA12p14611.

Maruyama, T., and N. Matuura (1984), Longitudinal variability of annual changes in activity of equatorial spread *F* and plasma bubbles, *J. Geophys. Res.*, *89*(A12), 10,903–10,912, doi:10.1029/JA089iA12p10903.

Mendillo, M., and J. Baumgardner (1982), Airglow characteristics of equatorial plasma depletions, *J. Geophys. Res.*, *87*(A9), 7641–7652, doi:10.1029/JA087iA09p07641.

Muralikrishna, P., and M. A. Abdu (2006), Rocket measurements of ionospheric electron density from Brazil in the last two decades, *Adv. Space Res.*, *37*, 1091–1096, doi:10.1016/j.asr.2006.02.006.

Pautet, P.-D., M. J. Taylor, N. P. Chapagain, H. Takahashi, A. F. Medeiros, F. T. Sao Sabbas, and D. C. Fritts (2009), Simultaneous observations of equatorial *F* region plasma depletions over Brazil during the Spread *F* Experiment (SpreadFEx), *Ann. Geophys.*, *27*, 2371–2381, doi:10.5194/angeo-27-2371-2009.

Pimenta, A. A., P. R. Fagundes, J. A. Bittencourt, Y. Sahai, D. Gobbi, A. F. Medeiros, M. J. Taylor, and H. Takahashi (2001), Ionospheric plasma bubble zonal drift: A methodology using OI (630.0 nm) all-sky imaging systems, *Adv. Space Res.*, *27*, 1219–1224, doi:10.1016/S0273-1177(01)00201-0.

Pimenta, A. A., J. A. Bittencourt, Y. Sahai, R. A. Buriti, H. Takahashi, and M. J. Taylor (2003a), Ionospheric plasma bubble zonal drifts over the tropical region: A study using OI (630.0 nm) emission all-sky images, *J. Atmos. Sol. Terr. Phys.*, *65*, 1117–1126, doi:10.1016/S1364-6826(03)00149-4.

Pimenta, A. A., P. R. Fagundès, Y. Sahai, J. A. Bittencourt, and J. R. Abalde (2003b), Equatorial *F* region plasma depletion drifts: Latitudinal and seasonal variations, *Ann. Geophys.*, *21*, 2315–2322, doi:10.5194/angeo-21-2315-2003.

Rohrbaugh, R. P., W. B. Hanson, B. A. Tinsley, B. L. Cragin, and J. P. McClure (1989), Images of trans-equatorial bubbles based on field-aligned airglow observations from Haleakala in 1984–1986, *J. Geophys. Res.*, *94*(A6), 6763–6770, doi:10.1029/JA094iA06p06763.

Sagawa, E., T. Maruyama, T. J. Immel, H. U. Frey, and S. B. Mende (2003), Global view of the nighttime low-latitude ionosphere by the IMAGE/FUV 135.6 nm observations, *Geophys. Res. Lett.*, *30*(10), 1534, doi:10.1029/2003GL017140.

Sahai, Y., J. Aarons, M. Mendillo, J. Baumgardner, J. A. Bittencourt, and H. Takahashi (1994), OI (630.0 nm) imaging observations of equatorial plasma depletions at 16°S dip latitude, *J. Atmos. Terr. Phys.*, *56*, 1461–1475, doi:10.1016/0021-9169(94)90113-9.

Taylor, M. J., and F. J. Garcia (1995), A two-dimensional spectral analysis of short period gravity waves imaged in the OI (557.7 nm) and near

infrared OH nightglow emissions over Arecibo, Puerto Rico, *Geophys. Res. Lett.*, *22*, 2473–2476, doi:10.1029/95GL02491.

Taylor, M. J., M. B. Bishop, and V. Taylor (1995), All-sky measurements of short period waves imaged in the OI (557.7 nm), Na (589.2 nm) and near infrared OH and O_2(0,1) nightglow emissions during the ALOHA-93 campaign, *Geophys. Res. Lett.*, *22*, 2833–2836, doi:10.1029/95GL02946.

Taylor, M. J., J. V. Eccles, J. LaBelle, and J. H. A. Sobral (1997), High resolution OI (630 nm) image measurements of *F* region depletion drifts during the Guára campaign, *Geophys. Res. Lett.*, *24*, 1699–1702, doi:10.1029/97GL01207.

Tinsley, B. A., R. P. Rohrbaugh, W. B. Hanson, and A. L. Broadfoot (1997), Images of trans-equatorial *F* region bubbles in 630 and 777 nm emissions compared with satellite measurements, *J. Geophys. Res.*, *102* (A2), 2057–2077, doi:10.1029/95JA01398.

Tsunoda, R. T., R. C. Livingston, J. P. McClure, and W. B. Hanson (1982), Equatorial plasma bubbles: Vertically elongated wedges from bottomside *F* layer, *J. Geophys. Res.*, *87*(A11), 9171–9180, doi:10.1029/JA087iA11p09171.

Valladares, C. E., J. W. Meriwether, R. Sheehan, and M. A. Biondi (2002), Correlative study of neutral winds and scintillation drifts measured near the magnetic equator, *J. Geophys. Res.*, *107*(A7), 1112, doi:10.1029/2001JA000042.

Weber, E. J., J. Buchau, R. H. Eatther, and S. B. Mende (1978), North-south aligned equatorial airglow depletions, *J. Geophys. Res.*, *83*(A2), 712–716, doi:10.1029/JA083iA02p00712.

Woodman, R. F. (1972), East-west ionospheric drifts at the magnetic equator, *Space Res.*, *81*, 5447–5466.

Yao, D., and J. J. Makela (2007), Analysis of equatorial plasma bubble zonal drift velocities in the Pacific sector by imaging techniques, *Ann. Geophys.*, *25*, 701–709, doi:10.5194/angeo-25-701-2007.

N. P. Chapagain and M. J. Taylor, Center for Atmospheric and Space Sciences, Utah State University, Logan, UT 84322, USA. (npchapagain@gmail.com)

J. V. Eccles, Space Science Environment Corporation, 221 N. Spring Creek Pkwy., Ste. A, Providence, UT 84332, USA.